# FPGA-Based Sensorless PMSM Speed Control Using Reduced-Order Extended Kalman Filters

Nguyen Khanh Quang, Nguyen Trung Hieu, and Q. P. Ha, *Senior Member, IEEE*

***Abstract*—This paper presents the design and implementation of a field-programmable gate array (FPGA)-based architecture for the speed control of sensorless permanent-magnet synchronous motor (PMSM) drives. For the reduction of computation resources, as well as accuracy improvement in the rotor position estimation, a parallel reduced-order extended Kalman filter (EKF) is proposed in this work. Compared with an EKF, the system order is reduced and the iteration process is greatly simplified, resulting in significant savings of resource utility, while maintaining high estimation performance. The whole control system includes a current-control-and-coordinate-transformation unit, a proportional–integral (PI) speed controller, and other accessory modules, all implemented in a single FPGA chip. A hardware description language is adopted to describe advantageous features of the proposed control system. Moreover, the finite-state-machine method is applied with the purpose to reduce logic elements used in the FPGA chip. The validity of the approach is verified through simulation based on the Modelsim/Simulink cosimulation method. Finally, experimental results are obtained on an FPGA platform with an inverter-fed PMSM to show the feasibility and effectiveness of the proposed system-on-programmable-chip for PMSM drives.**

***Index Terms*—Extended Kalman filter (EKF), field-programmable gate array (FPGA), permanent-magnet synchronous motor (PMSM) drive, sensorless control.**

## I. Introduction

Owing to the advantages of superior power density, high performance motion control with fast speed, and enhanced accuracy, the permanent-magnet synchronous motor (PMSM) has been increasingly used in robotics, precision machining, and many automation processes. In most real-world applications, conventional motor control needs a position sensor or an optical encoder to measure the rotor position for feedback to the controller to ensure the speed control precision. However, a position sensor presents some disadvantages affecting the cost, reliability, and noise immunity and is subject to such conditions like humidity and corrosion [1]. In recent years, the sensorless control of PMSM drives has become an important topic, and various sensorless control strategies have been investigated [2]–[6]. In sensorless control, the estimation of the rotor position and speed can be achieved by using an algorithmic estimator to alleviate the need of physical sensors. Available sensorless techniques are mainly classified into two different types: the high frequency (HF) injection method and the estimation-based techniques. The HF signal injection method, using the zero crossing of the silent phase's back electromotive force (EMF) of the motor to detect its rotor position, is more suitable for low-speed operations. In this method, the HF signal may bring noise to the system to degrade its performance, and its real-time implementation would need some special hardware support [7]–[10]. The rotor position estimation can be achieved via extended Luenberger state observers [11] or nonlinear observers where the estimation error is driven to zero using the principles of, for example, sliding modes, Kalman filtering, or a model reference adaptive system (MRAS). For the sensorless drive technology, while a sliding-mode observer (SMO) [12]–[14] may suffer from the chattering effect and the MRAS estimator [9] may have a difficulty in the parameter adaptation, an extended Kalman filter (EKF) [15]–[18], which is a nonlinear version for the recursive stochastic optimal Kalman filter, can be used for the estimation of the joint state and parameters as well as unknown disturbances in noisy environments. However, as remarked in [19], an EKF requires heavy online matrix computing, and the complex computation becomes a challenge for a fixed-point processor system, particularly for implementation on a field-programmable gate array (FPGA) chip. In [20], an EKF is implemented with a floating point digital signal processor (DSP), and the influence of its parameters on the outcomes of PMSM speed drives is studied. While floating point DSPs can perform complicated computations, they are not cost-effective PMSM speed drives. Moreover, a DSP tends to exhaust CPU resources and suffers from a poor timing performance [21]–[23].

Recently, manifesting the advantages of high reliability, low energy consumption, parallel processing, and fast time to market, the FPGA technology has been an attractive solution for embedded systems, motor drive, image processing, or robotics (see, e.g., [23]–[26]). The technology has brought forward the concept of system-on-programmable-chip to implement a highly complex control algorithm for motor drive systems [23], [27]–[29]. However, most on-chip programmable systems for motor drive applications have relied on systolic arrays to deal with the complicated computation of control algorithms [21]–[23], [25], [27]. Although systolic arrays, possessing the parallel processing capability, are ideal to implement on FPGAs with a fast execution time, their parallel architecture is quite complicated and requires much gate array resources.

Manuscript received July 15, 2013; revised October 28, 2013, January 21, 2014, and March 13, 2014; accepted March 31, 2014. Date of publication April 25, 2014; date of current version September 12, 2014.

N. K. Quang and Q. P. Ha are with the School of Electrical, Mechanical, and Mechatronic Systems, University of Technology Sydney, Ultimo, NSW 2007, Australia (e-mail: Quang.Nguyen@uts.edu.au; Quang.Ha@uts.edu.au).

N. T. Hieu is with the Laboratory of Network and Cyber Physical System, Institut National de la Recherche Scientifique, University of Quebec, Montreal, QC H5A 1K6, Canada; and also with Énergie Matériaux Télécommunications, University of Quebec, Varennes, QC J3X 1S2, Canada (e-mail: hieu.trung.nguyen@emt.inrs.ca).

Color versions of one or more of the figures in this paper are available online at http://ieeexplore.ieee.org.

Digital Object Identifier 10.1109/TIE.2014.2320215

This paper aims to design and implement a fully FPGA-based sensorless control paradigm for PMSM drives that can ensure both a significant reduction in the required FPGA resources and a fast execution time. Focusing on the demonstration of the control-system-on-chip concept for sensorless PMSM drives with EKFs, the contribution of this paper includes the following: 1) the feasible development of an effective design procedure for the FPGA-based control of sensorless PMSM drives using parallel reduced-order EKFs with a substantial decrease in the resource usage and execution time and 2) the full hardware implementation of the estimation and control paradigm on a single FPGA chip. For this, we seek, on the one hand, to lessen the number of matrix calculations in our EKF algorithm [17] and to reduce the EKF order, as generally outlined in [30]. Here, by estimating the back EMF according to the stator current observed as state variables, the decoupling of the system equation can be obtained to facilitate a reduced-order EKF. On the other hand, a finite-state machine (FSM) is developed in this work to result in less logic gates used, leading to a faster processing time. The contribution of this paper is significant as it provides an effective solution for the exploitation of the FPGA advantages in power electronics and drive applications as well as a convincing demonstration of high quality estimation in terms of accuracy and robustness against noisy and/or perturbed currents for sensorless PMSM control. In order to verify the performance the proposed on-chip control system, the cosimulation method Modelsim/Simulink [31] is used for extensive simulation. Then, experimental validation on a PMSM is conducted using an Altera kit and laboratory instrumentation.

## II. System Description and Sensorless Speed Control with EKF

### A. PMSM Drive Model

The coupled and nonlinear model of PMSM under field orientation can be expressed in $d$–$q$ axes by

$$\begin{bmatrix} v_d \\ v_q \end{bmatrix} = \begin{bmatrix} r_s + sL_d & -\omega_e L_q \\ \omega_e L_q & r_s + sL_d \end{bmatrix} \begin{bmatrix} i_d \\ i_q \end{bmatrix} + \left\{ (L_d - L_q)(-\omega_e i_d - \dot{i}_q) + \omega_e \lambda_f \right\} \begin{bmatrix} 0 \\ 1 \end{bmatrix} \quad (1)$$

which can be retransformed to the $\alpha$–$\beta$ axes as follows:

$$\begin{bmatrix} v_\alpha \\ v_\beta \end{bmatrix} = \begin{bmatrix} r_s + sL_d & \omega_e(L_d - L_q) \\ -\omega_e(L_d - L_q) & r_s + sL_d \end{bmatrix} \begin{bmatrix} i_\alpha \\ i_\beta \end{bmatrix} + \left\{ (L_d - L_q)(-\omega_e i_d - \dot{i}_q) + \omega_e \lambda_f \right\} \begin{bmatrix} -\sin\theta_e \\ \cos\theta_e \end{bmatrix} \quad (2)$$

where $[v_d\ v_q]^T$ and $[i_d\ i_q]^T$ are respectively the vectors of voltage and current in rotating coordinates, $[v_\alpha\ v_\beta]^T$ and $[i_\alpha\ i_\beta]^T$ are respectively those vectors in fixed coordinates, $r_s$ is the phase winding resistance, $L_d$ and $L_q$ are respectively the $d$ and $q$ axis inductances, $\omega_e$ is the rotating speed, $\lambda_f$ is the permanent-magnet flux linkage, and $\theta_e$ is correspondingly the rotor's angular position at that magnet flux.

This model is useful and can be applied to any type of synchronous motors such as the surface-mounted PMSM when $(L_d = L_q)$ or the interior PMSM when $(L_d < L_q)$.

### B. Extended Kalman Filter Algorithm

Kalman filtering is an optimal stochastic approach to state estimation and filtering in linear systems. For nonlinear systems, the state space equation can be written in the following form:

$$\dot{x}(t) = f\left(x(t)\right) + Bu(t) + \sigma(t) \quad (3)$$

$$y(t) = h\left(x(t)\right) + \mu(t) \quad (4)$$

where $x(t)$, $u(t)$, and $y(t)$ are respectively the system's state, input, and output. The system noise $\sigma(t)$ and measurement noise $\mu(t)$ are assumed to be zero mean and white with Gaussian distributions of covariances $Q(t)$ and $R(t)$, respectively. Once a nominal solution to the nonlinear (3) and (4) has been obtained, the linearized perturbation equations of the system are

$$\delta\dot{x}(t) = F\left(x(t)\right)\delta x(t) + B\delta u(t) + \sigma(t) \quad (5)$$

$$\delta y(t) = H\left(x(t)\right)\delta x(t) + \mu(t) \quad (6)$$

where the Jacobian and output matrices are defined respectively as follows:

$$F\left(x(t)\right) = \left.\frac{\partial f}{\partial x}\right|_{x=x(t)} \quad (7)$$

$$H\left(x(t)\right) = \left.\frac{\partial h}{\partial x}\right|_{x=x(t)}. \quad (8)$$

After discretization with a sampling period $T_c$, (5) becomes

$$x(t_n) = \Phi\left(t_n, t_{n-1}, x(t_{n-1})\right)x(t_{n-1}) + \left(\int_{t_{n-1}}^{t_n} \Phi\left(t_n, t_{n-1}, x(t_{n-1})\right) B d\tau\right) u(t_{n-1}) + \nu(t_{n-1}) \quad (9)$$

where the computation of the state transition matrix for system (5), $\Phi(t_n, t_{n-1}, x(t_{n-1}))$, can be simplified by the Euler approximation

$$\Phi\left(t_n, t_{n-1}, x(t_{n-1})\right) \cong I + FT_c \quad (10)$$

$$\int_{t_{n-1}}^{t_n} \Phi\left(t_n, t_{n-1}, x(t_{n-1})\right) B d\tau \cong BT_c. \quad (11)$$

Therefore, the discrete model of (5)–(8) becomes approximately

$$x(t_n) = (I + FT_c)x(t_{n-1}) + BT_c u(t_{n-1}) + \nu(t_{n-1}) \quad (12)$$

$$y(t_n) = Hx(t_n) + \xi(t_n) \quad (13)$$

where $\nu(t_n)$ and $\xi(t_n)$ are the discrete forms of system noise, with covariance $Q_d(t_n)$, and measurement noise, with covariance $R_d(t_n)$, respectively. The EKF is an optimal estimator which minimizes the cost function $J = \sum_{n=1}^{m} E\{\tilde{x}^2(n)\}$ in the least square sense, in which $\tilde{x}(n)$ is defined by the difference between the system state $x(n)$ and its estimate $\hat{x}(n)$, i.e., $\tilde{x}(n) = x(n) - \hat{x}(n)$. Accordingly, the EKF algorithm can be described by the following two-step recursive equations.

1) *Prediction*: The predicted estimate is obtained from (5) and by using a simple rectangular integration as

$$\hat{x}_{n|n-1} = \hat{x}_{n-1} + (F(\hat{x}_{n-1}) + B.u_{n-1})\,T_c \tag{14}$$

or from (12)

$$\hat{x}_{n|n-1} = (I + FT_c)\hat{x}_{n-1} + BT_c.u_{n-1}. \tag{15}$$

The estimate covariance is predicted by

$$P_{n|n-1} = \Phi_{n-1}P_{n-1}\Phi_{n-1}^T + Q_d. \tag{16}$$

2) *Updating*: From (6) and by using a simple rectangular integration, the updated estimate and, correspondingly, its covariance are obtained as

$$\hat{x}_n = \hat{x}_{n|n-1} + K_n(y_n - H\hat{x}_{n|n-1}) \tag{17}$$

$$P_n = P_{n|n-1} - K_nHP_{n|n-1} \tag{18}$$

where the Kalman gain is calculated by

$$K_n = P_{n|n-1}H^T(HP_{n|n-1}H^T + R_d)^{-1}. \tag{19}$$

In EKF, the linearization may cause the filter algorithm to quickly diverge while the computational cost for its realization increases drastically with the system complexity. A two-stage Kalman estimator could be used to reduce the number of arithmetic operations [32]. Here, motivated by the work in [15], the problem is addressed via a reduction in the system order by using two parallel EKFs [33], in order to meet the limited computational resources and processing time of FPGA implementation.

## III. Parallel Reduced-Order EKFs for Sensorless PMSM Drive

### A. PMSM Decoupled Dynamics

The circuit equation of PMSMs in (2) is rewritten on the $\alpha$–$\beta$ fixed coordinates as

$$\begin{bmatrix} v_\alpha \\ v_\beta \end{bmatrix} = \begin{bmatrix} r_s + sL_s & 0 \\ 0 & r_s + sL_s \end{bmatrix} \begin{bmatrix} i_\alpha \\ i_\beta \end{bmatrix} + \omega_e\lambda_f \begin{bmatrix} -\sin\theta_e \\ \cos\theta_e \end{bmatrix} \tag{20}$$

where $L_s \triangleq L_d = L_q$ and $s$ is the differential operator. In addition, let us define the EMF as

$$e = \begin{bmatrix} e_\alpha \\ e_\beta \end{bmatrix} \triangleq \omega_e\lambda_f \begin{bmatrix} -\sin\theta_e \\ \cos\theta_e \end{bmatrix}. \tag{21}$$

This basic EMF model is time varying in practice, and from the assignment of $\alpha$–$\beta$ coordinates, it can be incorporated in (20) to form the following dynamics:

$$\frac{d}{dt}\begin{bmatrix} i_\alpha \\ i_\beta \\ e_\alpha \\ e_\beta \end{bmatrix} = \begin{bmatrix} \frac{-r_s}{L_s} & 0 & \frac{-1}{L_s} & 0 \\ 0 & \frac{-r_s}{L_s} & 0 & \frac{-1}{L_s} \\ 0 & 0 & 0 & -\omega_e \\ 0 & 0 & \omega_e & 0 \end{bmatrix} \begin{bmatrix} i_\alpha \\ i_\beta \\ e_\alpha \\ e_\beta \end{bmatrix} + \begin{bmatrix} \frac{1}{L_s} & 0 \\ 0 & \frac{1}{L_s} \\ 0 & 0 \\ 0 & 0 \end{bmatrix} \begin{bmatrix} v_\alpha \\ v_\beta \end{bmatrix}. \tag{22}$$

To achieve the order reduction purpose, model (22) can be decoupled according to currents $i_\alpha$ and $i_\beta$ into

$$\frac{d}{dt}\begin{bmatrix} i_\alpha \\ e_\alpha \\ e_\beta \end{bmatrix} = \begin{bmatrix} \frac{-r_s}{L_s} & \frac{-1}{L_s} & 0 \\ 0 & 0 & -\omega_e \\ 0 & \omega_e & 0 \end{bmatrix} \begin{bmatrix} i_\alpha \\ e_\alpha \\ e_\beta \end{bmatrix} + \begin{bmatrix} \frac{1}{L_s} \\ 0 \\ 0 \end{bmatrix} [v_\alpha] \tag{23}$$

$$\frac{d}{dt}\begin{bmatrix} i_\beta \\ e_\beta \\ e_\alpha \end{bmatrix} = \begin{bmatrix} \frac{-r_s}{L_s} & \frac{-1}{L_s} & 0 \\ 0 & 0 & \omega_e \\ 0 & -\omega_e & 0 \end{bmatrix} \begin{bmatrix} i_\beta \\ e_\beta \\ e_\alpha \end{bmatrix} + \begin{bmatrix} \frac{1}{L_s} \\ 0 \\ 0 \end{bmatrix} [v_\beta]. \tag{24}$$

Thus, the dynamic models of the PMSM in the state variable form can be expressed generally as

$$\dot{x}(t) = Ax(t) + Bu(t) \tag{25}$$

$$y = Cx(t) \tag{26}$$

where $x(t) = [i_\alpha\ e_\alpha\ e_\beta]^T$, $y(t) = [i_\alpha]$, and $u(t) = [v_\alpha]$ or $x(t) = [i_\beta\ e_\beta\ e_\alpha]^T$, $y(t) = [i_\beta]$, and $u(t) = [v_\beta]$, respectively, in which the system matrices are given by

$$A = \begin{bmatrix} \frac{-r_s}{L_s} & \frac{-1}{L_s} & 0 \\ 0 & 0 & \mp\omega_e \\ 0 & \pm\omega_e & 0 \end{bmatrix},\ B = \begin{bmatrix} \frac{1}{L_s} \\ 0 \\ 0 \end{bmatrix},\ C = [\,1 \quad 0 \quad 0\,].$$

### B. Parallel Reduced-Order EKFs

To proceed with the EKF design, the Jacobian, output matrix, and state transition matrix are obtained respectively in accordance with (7), (8), and (10) as

$$F = \left.\frac{\partial f}{\partial x}\right|_{x=x(t)} = A = \begin{bmatrix} \frac{-r_s}{L_s} & \frac{-1}{L_s} & 0 \\ 0 & 0 & \mp\omega_e \\ 0 & \pm\omega_e & 0 \end{bmatrix} \tag{27}$$

$$H = \left.\frac{\partial h}{\partial x}\right|_{x=x(t)} = C = [\,1 \quad 0 \quad 0\,] \tag{28}$$

$$\Phi(t_n, t_{n-1}, x(t_n)) \cong I + FT_c = \begin{bmatrix} 1 - \frac{r_sT_c}{L_s} & \frac{-T_c}{L_s} & 0 \\ 0 & 1 & \mp\omega_eT_c \\ 0 & \pm\omega_eT_c & 1 \end{bmatrix} \triangleq \begin{bmatrix} \phi_1 & \phi_2 & 0 \\ 0 & 1 & \phi_3 \\ 0 & -\phi_3 & 1 \end{bmatrix}. \tag{29}$$

In our sensorless control scheme, according to the parity of the index $n$ of the sampling time $t_n$, currents $i_\alpha$ and $i_\beta$ are predicted/updated in subsequent samples, making use of the

time continuity of the inductive current. Then, the previous data of the rotor speed and EMF components $e_\alpha$ and $e_\beta$ are applied to two corresponding third-order EKFs in the prediction/updating steps to obtain the estimates $\hat{e}_\alpha$ and $\hat{e}_\beta$. Hence, operating at a time is only the EKF of the third order $(p = 3)$, instead of the fourth order $(p = 4)$. This therefore reduces the number of arithmetic operations involved and saves the logic elements (LEs) used. Thus, the estimated angular position $\hat{\theta}_e$ and rotor speed $\hat{\omega}_e$ to be used in the next step are obtained by the following equations:

$$\hat{\theta}_e(n) = \tan^{-1}\left(\frac{-\hat{e}_\alpha(n)}{\hat{e}_\beta(n)}\right) \tag{30}$$

$$\hat{\omega}_e(n) = \frac{1}{\lambda_f}\sqrt{\hat{e}_\alpha^2(n) + \hat{e}_\beta^2(n)}. \tag{31}$$

### C. Design Procedure

Step 1: Set the initial values of $Q_d$, $R_d$, $P_o$, and $n = 1$.

Step 2: Measure the values of $i_\alpha(n)$, $i_\beta(n)$, $v_\alpha(n)$, and $v_\beta(n)$ from the PMSM drive.

Step 3: Predict the temporary state variables by using (15). In particular, the scalar form of the prediction equation can be obtained from (22) as follows:

$$\hat{i}_\alpha(n|n-1) = \left(1 - \frac{r_s}{L_s}T_c\right)\hat{i}_\alpha(n-1) - \frac{T_c}{L_s}\hat{e}_\alpha(n-1) + \frac{T_c}{L_s}v_\alpha(n-1) \quad (\text{if } n \text{ is odd}) \tag{32}$$

$$\hat{i}_\beta(n|n-1) = \left(1 - \frac{r_s}{L_s}T_c\right)\hat{i}_\beta(n-1) - \frac{T_c}{L_s}\hat{e}_\beta(n-1) + \frac{T_c}{L_s}v_\beta(n-1) \quad (\text{if } n \text{ is even}) \tag{33}$$

$$\hat{e}_\alpha(n|n-1) = \hat{e}_\alpha(n-1) - \hat{\omega}_e(n-1)T_c\hat{e}_\beta(n-1) \tag{34}$$

$$\hat{e}_\beta(n|n-1) = \hat{e}_\beta(n-1) + \hat{\omega}_e(n-1)T_c\hat{e}_\alpha(n-1). \tag{35}$$

Step 4: Obtain the temporary covariance matrix $P_{n|n-1}$ from (16), where $\Phi_{n-1}$ is given by (29). Due to its symmetry, positive-definite matrix $P_{n|n-1}$ is chosen in the following form:

$$P_{n|n-1} = \begin{bmatrix} P_{11} & P_{21} & P_{31} \\ P_{21} & P_{22} & P_{23} \\ P_{31} & P_{23} & P_{33} \end{bmatrix}. \tag{36}$$

Step 5: Compute the Kalman gain (19) for the reduced-order filter by using (28) and (36) as

$$K_n = \begin{bmatrix} P_{11} \\ P_{21} \\ P_{31} \end{bmatrix} ([P_{11}] + R_d)^{-1} = \begin{bmatrix} P_{11} \\ P_{21} \\ P_{31} \end{bmatrix} [T_{11}]^{-1} \triangleq \begin{bmatrix} k_{11} \\ k_{21} \\ k_{31} \end{bmatrix}. \tag{37}$$

Step 6: Update the predicted state variables from (17) for the following cases:

(i) $n$ is odd

$$\hat{i}_\alpha(n) = \hat{i}_\alpha(n|n-1) + k_{11}\tilde{i}_\alpha(n) \tag{38}$$

$$\hat{e}_\alpha(n) = \hat{e}_\alpha(n|n-1) + k_{21}\tilde{i}_\alpha(n) \tag{39}$$

$$\hat{e}_\beta(n) = \hat{e}_\beta(n|n-1) + k_{31}\tilde{i}_\alpha(n). \tag{40}$$

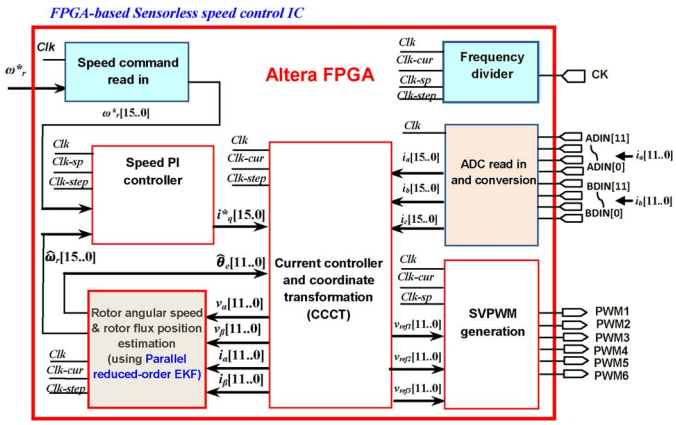


Fig. 1. Proposed sensorless speed control IC circuitry.

TABLE I
COMPLEXITY OF EKF ALGORITHMS

| | Full-order EKF($p$=4) | Reduced-order EKF($p$=3) |
|---|---|---|
| Multiplications | 94 | 32 |
| Additions | 67 | 21 |
| Subtractions | 31 | 8 |
| Divisions | 7 | 4 |

(ii) $n$ is even

$$\hat{i}_\beta(n) = \hat{i}_\beta(n|n-1) + k_{11}\tilde{i}_\beta(n) \tag{41}$$

$$\hat{e}_\beta(n) = \hat{e}_\beta(n|n-1) + k_{21}\tilde{i}_\beta(n) \tag{42}$$

$$\hat{e}_\alpha(n) = \hat{e}_\alpha(n|n-1) + k_{31}\tilde{i}_\beta(n) \tag{43}$$

where

$$\tilde{i}_\alpha(n) = i_\alpha(n) - \hat{i}_\alpha(n|n-1) \tag{44}$$

$$\tilde{i}_\beta(n) = i_\beta(n) - \hat{i}_\beta(n|n-1) \tag{45}$$

in which $k_{ij}$ are elements of the Kalman gain $K_n$.

Step 7: Update the present covariance matrix $P_n$ from (18).

Step 8: Compute the rotor angular speed and rotor flux position from (30) and (31). Then, set $n = n + 1$, and go back to *Step 2*.

## IV. FPGA Control Architecture and FSM Implementation

### A. FPGA Architecture for Sensorless PMSM Speed Control

Fig. 1 shows the FPGA-based architecture of the proposed speed control system for the sensorless PMSM drive. The control system includes a PI speed controller, a speed command read-in unit, a current control and coordinate transformation (CCCT) module, a space vector pulsewidth modulation (SVPWM) generator, a quadrature-encoder-pulse detection and transformation module, an analog-to-digital converter (ADC) read-in and conversion, a frequency divider, and a parallel reduced-order EKF-based rotor flux angle and rotor speed estimation module. All modules are described by the very high speed hardware description language (VHDL) and simulated in Modelsim to test their feasibility before implementation in

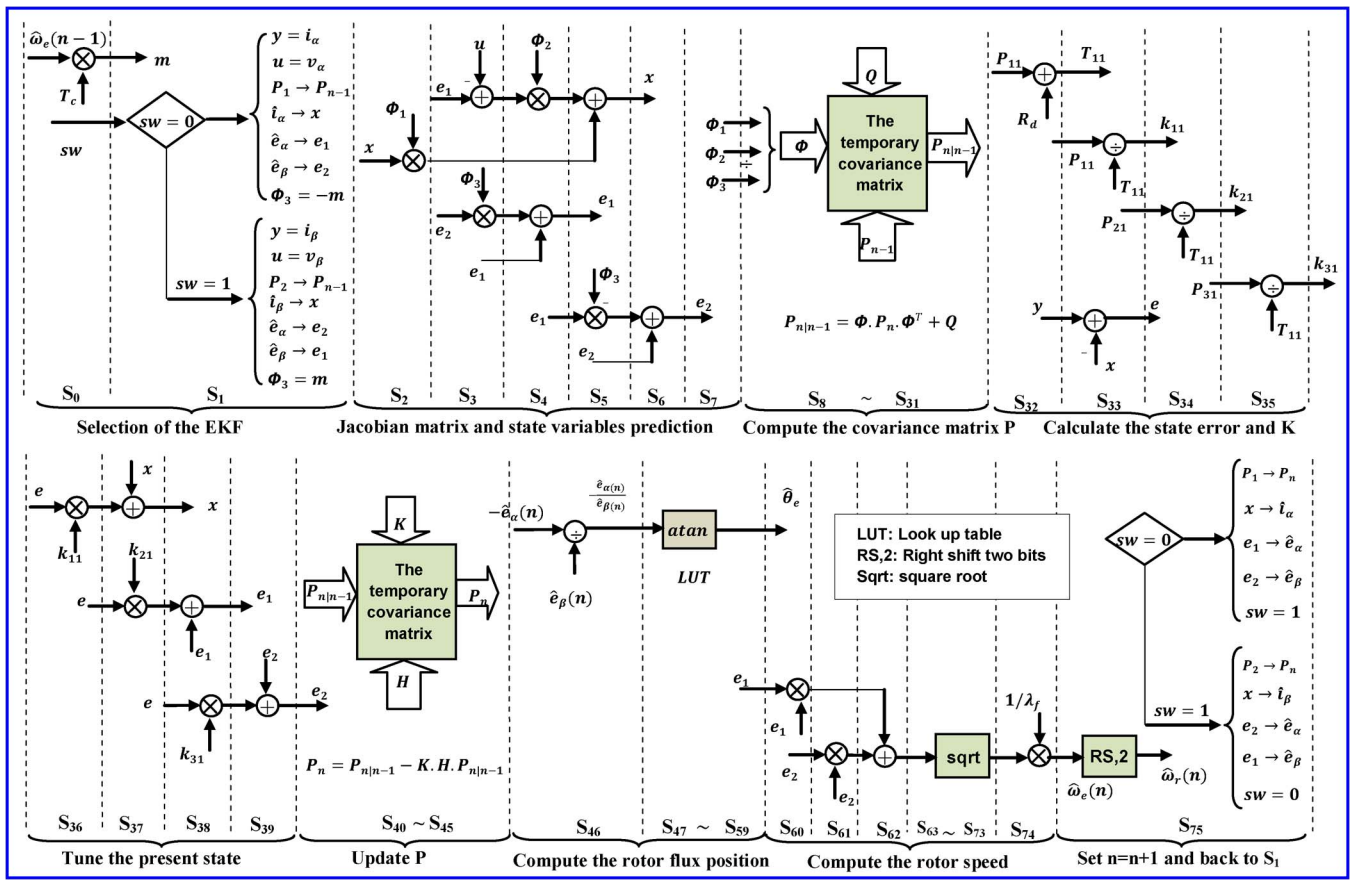


Fig. 2. State machine diagram of the parallel reduced-order EKF algorithm.

Altera Cyclone II EP2C70. The sampling frequency for the current and speed controllers is designated at 16 and 2 kHz, respectively. The operating clock rate of the designed FPGA controller is 50 MHz, and the frequency divider generates 50 MHz (*Clk*), 12.5 MHz (*Clk-step*), 16 kHz (*Clk-cur*), and 2 kHz (*Clk-sp*) clocks to supply all module circuits of the application system-on-chip.

### B. EKF Complexity and Implementation With FSM

The computational cost for EKF realization increases drastically with the algorithm complexity. In our approach, this has been significantly reduced owing to a decrease in the system order by using two parallel EKFs. The complexity, in terms of the number of arithmetic operations, for the full-order EKF ($p = 4$) and proposed reduced-order EKF ($p = 3$) is evaluated in Table I.

For implementation, an FSM is employed to describe the parallel reduced-order EKF algorithm, as shown in Fig. 2, where the data type adopts a 16-b length with Q15 format and 2's complement operations. Although the EKF algorithm described is complex, the FSM adequately incorporates the control structure and can be described by VHDL. Here, the divider, multiplier, and adder apply the Altera Library Parameterized Modules standard. It manipulates a 75-step machine to carry out the overall computations.

In our FSM, steps $S_0 - S_1$ select one of the two EKFs, steps $S_2 - S_7$ execute the computation of the Jacobian matrix and predicted state variables, steps $S_8 - S_{31}$ are for the calculation of the temporary covariance matrix, steps $S_{32} - S_{35}$ describe the computation of the state error and the Kalman gain $K_n$, steps $S_{36} - S_{39}$ perform the present state updating, steps $S_{40} - S_{45}$ update the present covariance matrix $P_n$, steps $S_{46} - S_{59}$ compute the rotor flux position, steps $S_{40} - S_{45}$ compute the rotor speed, and finally, step $S_{75}$ is for getting back to step 1 for a new iteration loop. Since the execution of each step can be completed within 80 ns corresponding to the frequency of 12.5 MHz in FPGA, a total of $N_{\mathrm{EKF}} = 75$ steps needs 6 $\mu$s for the parallel reduced-order EKF operation. Similarly, the numbers of steps for the execution of CCCT and SVPWM are respectively $N_{\mathrm{CCCT}} = 24$ and $N_{\mathrm{SVPWM}} = 13$ steps. The total resource usage in FPGA is 5996 LEs, 5 hardwired (hw) 18-b multipliers, and 73 728 RAM bit resource for the Cyclone II EP2C70, as summarized in Table II.

TABLE II
FPGA UTILITY EVALUATION FOR SENSORLESS PMSM SPEED CONTROL

| Module circuits | LEs | Memory (bits) | hw 18-bit multipliers |
|---|---|---|---|
| 1. CCCT | 864 | 24,576 | 1 |
| 2. SVPWM generation | 1,221 | 0 | 1 |
| 3. ADC read-in and conversion | 136 | 0 | 1 |
| 4. Speed PI controller | 254 | 0 | 1 |
| 5. Parallel reduced-order EKF | 3,521 | 49,152 | 1 |
| **TOTAL** | **5,996** | **73,728** | **5** |

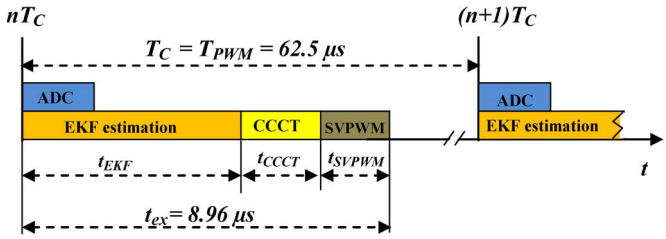


Fig. 3. Timing diagram of the sensorless control system.

### C. Sensorless Control Timing Diagram

The designed sampling interval is $T_c = 62.5\ \mu$s (16 kHz), the same as the pulse width modulation (PWM) switching period. Since all processes are implemented by using FSM, the execution time $t_{\rm ex}$ is calculated by

$$\begin{aligned} t_{\rm ex} &= t_{\rm EKF} + t_{\rm CCCT} + t_{\rm SVPWM} \\ &= (N_{\rm EKF} + N_{\rm CCCT} + N_{\rm SVPWM}).T_{Clk\text{-}step} \end{aligned} \tag{46}$$

where $T_{Clk\text{-}step}$, $t_{\rm EKF}$, $t_{\rm CCCT}$, and $t_{\rm SVPWM}$ are respectively the clock step period, execution time for reduced-order extended Kalman filtering, CCCT, and SVPWM. The ADC conversion and the divider, multiplier, and adder all use 50 MHz clock (*Clk*), and 12.5 MHz (*Clk-step*) is used for step implementation. Fig. 3 shows the timing diagram of all blocks in the FPGA-based sensorless control for PMSM using the proposed reduced-order EKFs.

At the beginning of the $n$th sampling period $nT_c$, the ADC read-in and conversion block reads and converts the values of the stator currents from two external ADCs (AD574AJN). This block is implemented by 80 steps and at 50 MHz clock, i.e., 1.6-$\mu$s operation time. At the same time, the EKF estimation is activated and generates the estimated position angle $\theta_e$ to CCCT and the estimated rotor speed to the speed control loop. The EKF estimation block is executed in 75 steps with 6 $\mu$s in total. The CCCT block, including the circuits of $d$ and $q$ axis PI control, transformation, and cosine/sine lookup table, operates sequentially with 24 steps at 12.5 MHz clock, resulting in an execution time of 1.92 $\mu$s. Its outputs are three-phase reference voltages $(v_{ref1}, v_{ref2}, v_{ref3})$, which are input to the SVPWM block, implemented by a state vector machine with a computation time of 1.04 $\mu$s for 13 steps.

The total execution time is $t_{\rm ex} = 8.96\ \mu$s. Although the FSM method needs more operation time, it consumes less FPGA resources than the parallel processing method.

## V. FPGA-Based Sensorless PMSM Drive Cosimulation

### A. Modelsim/Simulink Cosimulation

Simulation is performed by using the Electronic Design Automation Simulator Link, which provides a verification interface between MATLAB/Simulink and the VHDL simulator on an FPGA board (see, e.g., [24], [28], and [29]).

Five modules are created for a PI speed controller, CCCT and SVPWM units, and the rotor flux position estimator using either the proposed parallel reduced-order EKFs, full-order

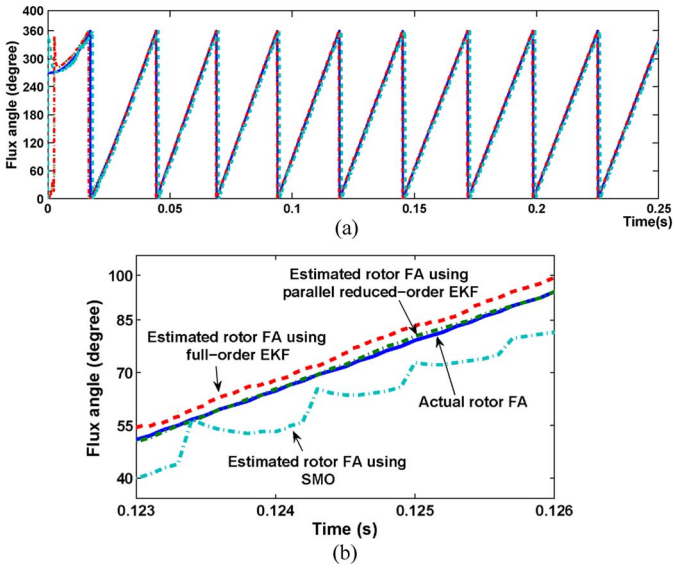


Fig. 4. Speed of 900 r/min. (a) Actual and estimated rotor flux angle from SMO, full-order EKF, and parallel reduced-order EKFs. (b) Zoom-in responses.

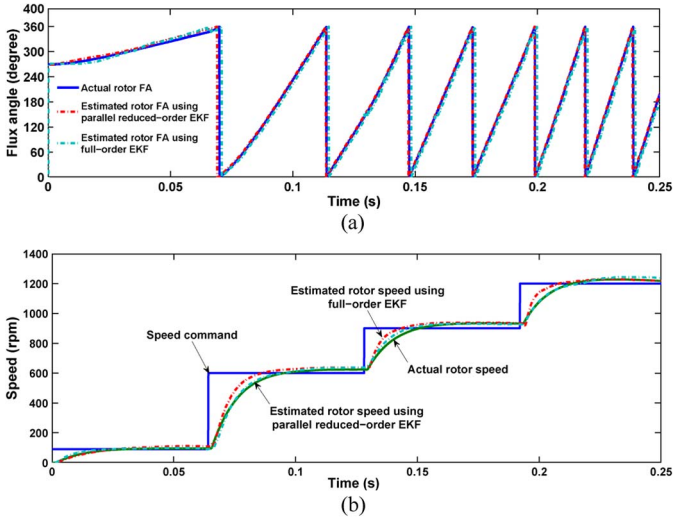


Fig. 5. Speed pattern $0 \rightarrow 90 \rightarrow 600 \rightarrow 900 \rightarrow 1200$ r/min. (a) Actual and estimated rotor flux angles and (b) actual and estimated speeds.

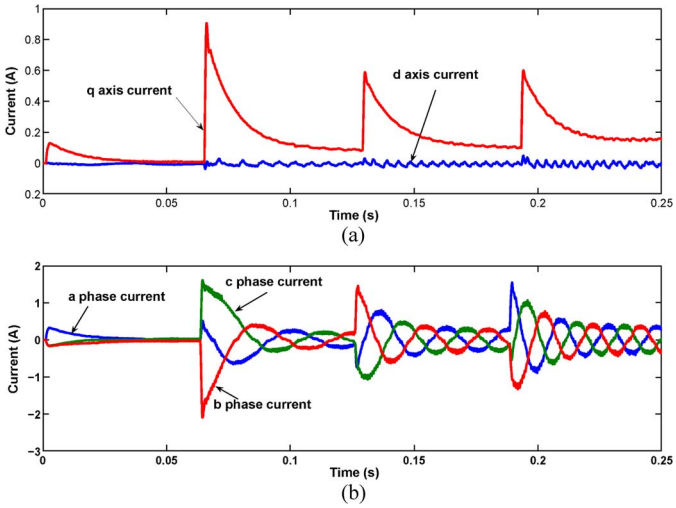


Fig. 6. Responses with reduced-order EKFs: (a) $d$–$q$ currents; and (b) three-phase currents.

TABLE III
HARDWARE RESOURCE CONSUMPTION AND EXECUTION TIME IN SENSORLESS CONTROL IMPLEMENTATION

| Sensorless techniques | Logic elements | Hardwired resources | Memory | Execution time ($\mu s$) |
|---|---|---|---|---|
| 1. SMO on EP2C70F896C6 | 4,626 (6.8%) | 5 hw 18-bit multipliers (3.3%) | 49,152 RAM bits (4%) | 5.84 |
| 2. Full-order EKF on EP2C70F896C6 | 6,633 (9.7%) | 5 hw 18-bit multipliers (3.3%) | 49,152 RAM bits (4%) | 13.36 |
| 3. Reduced-order EKF on EP2C70F896C6 | 5,996 (8.8%) | 5 hw 18-bit multipliers (3.3%) | 49,152 RAM bits (4%) | 8.96 |
| 4. Standard EKF on XC3S1600E [23]* | 7,376 (63%) | 36 hw 18-bit multipliers (100%) | 18,000 RAM bits (3%) | 6.82 |

* One configurable logic block of Xilinx is equivalent to two Altera logic elements (LEs)

EKF, or SMO, respectively. To be consistent with the hardware implementation, the sampling frequency of current and speed control is selected respectively as 16 and 2 kHz. The clocks of 50 MHz, 12.5 MHz, and 16 kHz supply to all other modules of Modelsim in accordance with the architecture of Fig. 1. The parameters of an eight-pole PMSM used in our simulation are as follows: $r_s = 1.3\ \Omega$, $L_s = 6.3$ mH, moment of inertia $J = 0.000108\ \text{kg} \cdot \text{m}^2$, and friction factor $B = 0.0013\ \text{N} \cdot \text{m} \cdot \text{s/rad}$.

### B. Estimation and Speed Control: Simulation Results

To show the effectiveness of the proposed parallel reduced-order EKF technique for sensorless PMSM control, we compare with cases using a full-order EKF and SMO with the same algorithm and estimator parameters as reported respectively in [23] and [29]. The simulation results are shown in Figs. 4–6. In Fig. 4(a), the actual rotor flux angle and its estimates are shown for a full-order EKF, SMO, and the proposed parallel reduced-order EKFs, typically at 900 r/min. Their zoom-in responses between 0.123 and 0.126 (s) are depicted in Fig. 4(b) to show the accuracy of the three estimation techniques. The estimated flux angle has a 3° phase error, about 150-$\mu$s delay time under a reference speed of 900 r/min by using the parallel reduced-order EKF method.

We then consider the case when the motor speed command is varied with a staircase pattern $90 \rightarrow 600 \rightarrow 900 \rightarrow 1200$ r/min using the full-order and parallel reduced-order EKFs. Fig. 5(a) and (b) show respectively the actual and estimated rotor flux angles and the actual and estimated speed responses for both EKF techniques. A slight improvement in the estimation performance with a rising time of 20 ms and steady-state error near 0 r/min is accounted for by the easy tuning of the filter parameters with a lower order. Responses of the currents are presented in Fig. 6(a) for the $d$–$q$ axes and in Fig. 6(b) for three phases when using the parallel reduced-order EKFs. The current responses are consistent with the staircase speed patterns applied to the sensorless PMSM.

### C. Resource Consumption and Execution Time Analysis

Table III summarizes the overall hardware resource consumption and execution time for the speed control of sensorless PMSM drives using low-cost Altera Cyclone II FPGA (EP2C70F896C6) with three different types of sensorless techniques mentioned earlier in comparison with another low-cost FPGA, the Xilinx Spartan 3E (XC3S1600E), reported in [23]. Hardware resource usage and execution time for the system with an EKF implementation are larger than for a SMO as it requires more matrix computations. However, simulation results

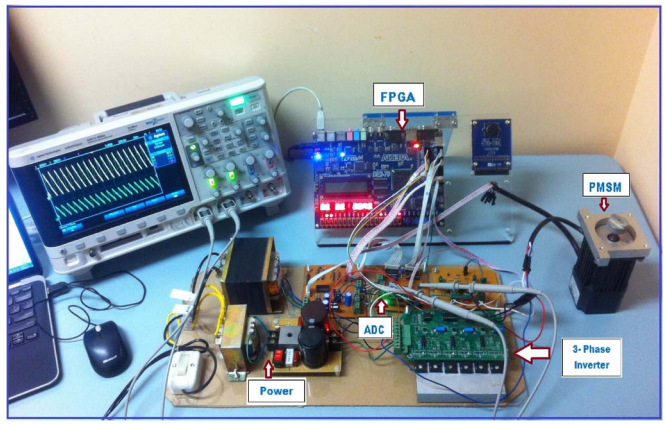


Fig. 7. Setup photograph.

show that EKFs yield better performance than SMO. It is clear from Fig. 4(b) that SMO has a larger error (9°) and slower response (400 $\mu$s) compared to the full-order EKF (5° and 250 $\mu$s) and our proposed method (2° and 150 $\mu$s). Compared with an FPGA-based standard EKF implementation using parallel processing systolic arrays, which are ideal to implement on FPGAs, the systolic array, albeit having a fast execution time, requires much FPGA resources, and its parallel architecture is quite complicated. The results given in [23], using the Xilinx Spartan 3E (XC3S1600E) with a 44-MHz clock frequency and 22-b format in the standard EKF, showed good control performance with 6.82 $\mu$s for execution owing to the parallel design methodology, but at high expenses of the computational resource with 7376 LEs, 18 000 RAM bits, and 36 hw 18-b multipliers. The proposed method has thus achieved a very good compromise between the hardware resource consumption (5996 LEs, 49 152 b, and 5 hw 18-b multipliers), execution time of 8.96 $\mu$s (with a 12.5-MHz clock frequency), and overall control performance of the system.

## VI. IMPLEMENTATION AND RESULTS

### A. Laboratory Setup

The on-chip control system and IGBT inverter voltage source supplied to the sensorless PMSM drive is depicted in a photograph shown in Fig. 7.

1) *Motor*: The PMSM's nameplate specifications are 100 W, four poles, 100 V, 1.7 A, and 3000 r/min. The brake torque of the motor is 0.32 N · m. It uses an optical encoder of 1000 pulses/rev.
2) *Supply*: The inverter has six sets of power transistors of the IGBT type. The collector-emitter voltage of the IGBT

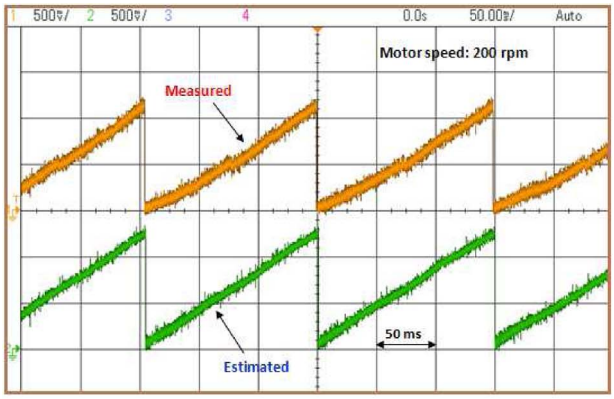


(a)

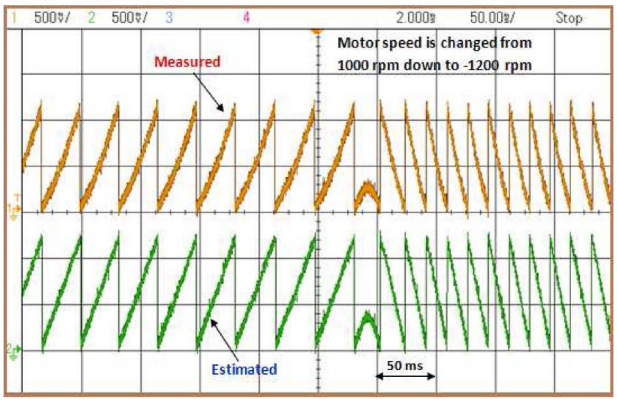


(b)

Fig. 8. Estimated and measured flux angles when PMSM is running at (a) 200 r/min and (b) from 1000 to −1200 r/min.

is rating 500 V, the gate-emitter voltage is rating ±20 V, and the collector current is rating 20 A in dc. Input signals of the inverter are PWM signals from the FPGA.

3) *On-chip control system*: The FPGA chip Cyclone II (EP2C70F896C6), produced by Altera, has 68 416 LEs, 1 152 000 b of on-chip RAM, 150 hw 18-b embedded multipliers, 36 DSP blocks, and maximum user I/O pins of 622.

### B. Experimental Results

For implementation, the PWM frequency, inverter dead-band interval, current loop sampling frequency, and speed loop sampling frequency are designated respectively at 16 kHz, 1 $\mu$s, 16 kHz, and 2 kHz. In the proposed sensorless control IC, the modules for current control, speed control, current vector control scheme, SVPWM generation, ADC read-in and conversion, coordinate transformation, and parallel reduced-order EKFs for rotor flux angle and rotor speed estimation are all realized by hardware in the FPGA chip. Again, the PMSM is experimentally tested at various speed commands. For verification, the encoder attached to the PMSM is used to obtain the actual rotor flux position. As shown in Fig. 8(a), at 200 r/min, the estimated flux angle exhibited around 4° phase error as compared with the measurements from the encoder sensor. When the PMSM reversed from 1000 to −1200 r/min, the estimated flux angle almost matched the actual value obtained from the encoder, as shown in Fig. 8(b). Experiment results indicate that the proposed parallel reduced-order EKFs for estimating the flux angle are suitable for a wide speed range of the motor, including a low speed, a moderate, or a high speed motor running in both forward and reverse directions. At a low speed of the motor, the weak back EMF signal tends to affect the accuracy of the flux position, but it is not considerable. At a speed command of 1000 r/min, the PMSM was loaded from a 2 N · m external load, and the step response using the proposed estimation method is shown in Fig. 9, where the rising time and steady-state error value are observed as 250 ms and near 0 r/min. Experimental results show that all the rotor tracks the electrical reference speed in different operation conditions of the PMSM. These together have confirmed the effectiveness and correctness of the proposed FPGA-based control architecture for sensorless PMSM drives.

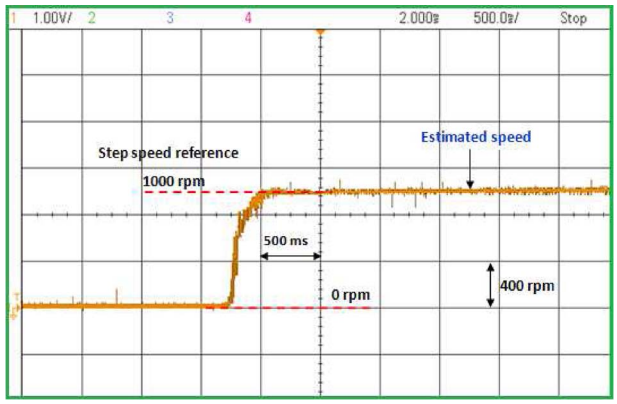


Fig. 9. Speed step response of the sensorless PMSM drive.

## VII. Conclusion

In this paper, we have presented a fully FPGA-based speed control system for a sensorless PMSM by using the parallel reduced-order EKFs for estimation and the FSM method for algorithm implementation. The proposed system comprises a PI speed controller, field-oriented PI current controllers, a rotor flux angle, and a rotor speed estimator together with other modules for command read-in, frequency divider, ADC conversion, and SVPWM generation. The whole system architecture has been successfully realized in one FPGA chip with a small resource usage as well as a fast execution time. The proposed flux angle and speed estimator algorithms have proven their effectiveness in the estimation of the rotor speed as verified by the cosimulation method and in extensive experiments. Simulation results have shown better performance when compared with other schemes for FPGA-based sensorless speed control in PMSM drives. Real-time responses obtained from a laboratorial setup with a Cyclone II FPGA platform are included for the performance validation of the control-system-on-programmable-chip design.

## References

[1] P. Tomei and C. M. Verrelli, "Observer-based speed tracking control for sensorless permanent magnet synchronous motors with unknown load torque," *IEEE Trans. Autom. Control*, vol. 56, no. 6, pp. 1484–1488, Jun. 2011.

[2] S. M. Gadoue, D. Giaouris, and J. W. Finch, "Sensorless control of induction motor drives at very low and zero speeds using neural network flux observers," *IEEE Trans. Ind. Electron.*, vol. 56, no. 8, pp. 3029–3039, Aug. 2009.
[3] Q. Zhou, P. Shi, S. Xu, and H. Li, "Observer-based adaptive neural network control for nonlinear stochastic systems with time delay," *IEEE Trans. Neural Netw. Learn. Syst.*, vol. 24, no. 1, pp. 71–80, Jan. 2013.
[4] S. Chi, Z. Zhang, and L. Y. Xu, "Sliding mode sensorless control of direct drive PM synchronous motors for washing machine applications," *IEEE Trans. Ind. Appl.*, vol. 45, no. 2, pp. 582–590, Mar./Apr. 2009.
[5] K. C. Veluvolu and Y. C. Soh, "High-gain observers with sliding mode for state and unknown input estimations," *IEEE Trans. Ind. Electron.*, vol. 56, no. 9, pp. 3386–3393, Sep. 2009.
[6] G. Foo and M. F. Rahman, "Sensorless sliding-mode MTPA control of an IPM synchronous motor drive using a sliding-mode observer and HF signal injection," *IEEE Trans. Ind. Electron.*, vol. 57, no. 4, pp. 1270–1278, Apr. 2010.
[7] A. Accetta, M. Cirrincione, M. Pucci, and G. Vitale, "Sensorless control of PMSM fractional horsepower drives by signal injection and neural adaptive-band filtering," *IEEE Trans. Ind. Electron.*, vol. 59, no. 3, pp. 1355–1366, Mar. 2012.
[8] R. Leidhold, "Position sensorless control of PM synchronous motors based on zero-sequence carrier injection," *IEEE Trans. Ind. Electron.*, vol. 58, no. 12, pp. 5371–5379, Dec. 2011.
[9] T. Orlowska-Kowalska and M. Dybkowski, "Stator-current-based MRAS estimator for a wide range speed-sensorless induction-motor drive," *IEEE Trans. Ind. Electron.*, vol. 57, no. 4, pp. 1296–1308, Apr. 2010.
[10] S. Bolognani, S. Calligaro, R. Petrella, and M. Tursini, "Sensorless control of IPM motors in the low-speed range and at standstill by HF injection and DFT processing," *IEEE Trans. Ind. Appl.*, vol. 47, no. 1, pp. 96–104, Jan./Feb. 2011.
[11] F. Poulain, L. Praly, and R. Ortega, "An observer for permanent magnet synchronous motors with currents and voltages as only measurements," in *Proc. 47th IEEE CDC*, Dec. 2008, pp. 5390–5395.
[12] K. Hongryel, S. Jubum, and L. Jangmyung, "A high-speed sliding-mode observer for the sensorless speed control of a PMSM," *IEEE Trans. Ind. Electron.*, vol. 58, no. 9, pp. 4069–4077, Sep. 2011.
[13] Q. Zhaowei *et al.*, "New sliding-mode observer for position sensorless control of permanent-magnet synchronous motor," *IEEE Trans. Ind. Electron.*, vol. 60, no. 2, pp. 710–719, Feb. 2013.
[14] M. Ezzat, A. Glumineau, and F. Plestan, "Sensorless high order sliding mode control of permanent magnet synchronous motor," in *Proc. 11th Int. Workshop VSS*, Jun. 2010, pp. 233–238.
[15] J. S. Jang, B. G. Park, T. S. Kim, D. M. Lee, and D. S. Hyun, "Parallel reduced-order extended Kalman filter for PMSM sensorless drives," in *Proc. 34th IEEE IECON/IECON*, Nov. 2008, pp. 1326–1331.
[16] K. Yoon-Ho and K. Yoon-Sang, "High performance IPMSM drives without rotational position sensors using reduced-order EKF," *IEEE Trans. Energy Convers.*, vol. 14, no. 4, pp. 868–873, Dec. 1999.
[17] W. Wenjie, Z. Min, and W. Qinghai, "Application of reduced-order extended Kalman filter in permanent magnet synchronous motor sensorless regulating system," in *Proc. IEEE ICDMA*, Dec. 2010, pp. 271–274.
[18] W. Wang, M. Zhang, and Q. Wu, "Application of reduced-order extended Kalman filter in permanent magnet synchronous motor sensorless regulating system," in *Proc. IEEE ICDMA*, Nov. 2010, pp. 271–274.
[19] M. Hilairet, F. Auger, and C. Darengosse, "Two efficient Kalman filters for flux and velocity estimation of induction motors," in *31st IEEE PESC/IEEE Power Electron. Spec. Conf.*, 2000, vol. 2, pp. 891–896.
[20] S. Bolognani, L. Tubiana, and M. Zigliotto, "Extended Kalman filter tuning in sensorless PMSM drives," *IEEE Trans. Ind. Appl.*, vol. 39, no. 6, pp. 1741–1747, Nov./Dec. 2003.
[21] L. Idkhajine, E. Monmasson, M. W. Naouar, A. Prata, and K. Bouallaga, "Fully integrated FPGA based controller for synchronous motor drive," *IEEE Trans. Ind. Electron.*, vol. 56, no. 10, pp. 4006–4017, Oct. 2009.
[22] E. Monmasson *et al.*, "FPGAs in industrial control applications," *IEEE Trans. Ind. Informat.*, vol. 7, no. 2, pp. 224–243, May 2011.
[23] L. Idkhajine, E. Monmasson, and A. Maalouf, "Fully FPGA-based sensorless control for synchronous ac drive using an extended Kalman filter," *IEEE Trans. Ind. Electron.*, vol. 59, no. 10, pp. 3908–3918, Oct. 2012.
[24] K. Ying-Shieh and T. Ming-Hung, "FPGA-based speed control IC for PMSM drive with adaptive fuzzy control," *IEEE Trans. Power Electron.*, vol. 22, no. 6, pp. 2476–2486, Nov. 2007.
[25] V. D. Colli, R. D. Stefano, and F. Marignetti, "A system-on-chip sensorless control for a permanent magnet synchronous motor," *IEEE Trans. Ind. Electron.*, vol. 57, no. 11, pp. 3822–3829, Nov. 2010.
[26] Q. P. Ha, Y.-H. Yu, and N. K. Quang, "FPGA-based cooperative control of indoor multiple robots," *Int. J. Adv. Mechatron. Syst.*, vol. 4, no. 5/6, pp. 248–259, 2012.
[27] L. Idkhajine and E. Monmasson, "Design methodology for complex FPGA-based controllers: Application to an EKF sensorless ac drive," in *Proc. IEEE 19th ICEM*, Sep. 2010, pp. 1–6.
[28] N. K. Quang, Y.-S. Kung, and Q. P. Ha, "FPGA-based control architecture integration for multiple-axis tracking motion systems," in *Proc. IEEE/SICE Int. Symp. SII*, Dec. 2011, pp. 591–596.
[29] N. K. Quang, N. D. That, N. H. Quang, and Q. P. Ha, "FPGA-based fuzzy sliding mode control for sensorless PMSM drive," in *Proc. IEEE Int. Conf. Autom. Sci. Eng.*, Aug. 2012, pp. 172–177.
[30] B. Saunders, G. Heins, and F. De Boer, "Framework for sensitivity analysis of industry algorithms for sensorless PMSM drives," in *Proc. 21st Australasian Conf. Univ. Power Eng.*, Sept. 2011, pp. 1–6.
[31] Y. Li *et al.*, "An open loop Sin microstepping driver based on FPGA and the co-simulation of Modelsim and Simulink," in *Proc. Int. Conf. CMCE*, Aug. 2010, pp. 223–227.
[32] M. Hilairet, F. Auger, and E. Berthelot, "Speed and rotor flux estimation of induction machines using a two-stage extended Kalman filter," *Automatica*, vol. 45, no. 8, pp. 1819–1827, Aug. 2009.
[33] N. K. Quang, N. T. Hieu, G. P. Hunter, and Q. P. Ha, "FPGA-based sensorless PMSM drive using parallel reduced-order extended Kalman filter," in *Proc. IEEE Int. Conf. Control, Autom. Inf. Sci.*, Nov. 2012, pp. 164–169.

**Nguyen Khanh Quang** received the B.S. degree in electrical engineering from the Danang University of Technology, Danang, Vietnam, in 2006, and the M.S. degree in electrical engineering from the Southern Taiwan University of Technology, Tainan, Taiwan, in 2010. He has been working toward the Ph.D. degree since July 2011 in the School of Electrical, Mechanical, and Mechatronic Systems, University of Technology Sydney, Ultimo, Australia.

His research interests include motion control, field-programmable-gate-array-based control, and estimation for motor drives applications.

**Nguyen Trung Hieu** received the B.S. degree in electrical engineering from the Hanoi University of Science and Technology, Hanoi, Vietnam, in 2010, and the M.S. degree in electrical engineering from the Southern Taiwan University of Science and Technology, Tainan, Taiwan, in 2012. He has been working toward the Ph.D. degree since January 2013 in the Institut National de la Recherche Scientifique, Universite du Quebec, Montreal, QC, Canada.

His research interests include field-programmable-gate-array-based design of controllers, and observers for drives applications and smart grids.

**Q. P. Ha** (SM'13) received the Ph.D. degree in electrical engineering from the Moscow Power Engineering Institute, Moscow, Russia, in 1993.

He is currently an Associate Professor with the School of Electrical, Mechanical, and Mechatronic System, University of Technology–Sydney, Ultimo, Australia. His research interests include automation, control, robotics, and computational intelligence.

Dr. Ha was an Associate Editor for the IEEE TRANSACTIONS ON AUTOMATION SCIENCE AND ENGINEERING (2009–2013), and is on the Board of Directors of the International Association of Automation and Robotics in Construction and the Editorial Board of Elsevier's Automation in Construction.